

1 The authors acknowledge two anonymous referees for their valuable suggestions. The
2 point-by-point revision notes are appended below. The revised part was highlighted
3 with red fonts in the main text of the revised manuscript.

4
5 **Replies to Anonymous Referee #1**

6
7 (1) Specific comments. 142: the word scalps is not clear to me. I consulted some English dictionaries and
8 the meaning I have found is not appropriated for the context. Please specify better what are you
9 describing.

10
11 The word “Scalps” was replaced with the landslide headscarp

12
13 (2) 210-212: an indication of the approximative value of the energy cut on muons and e.m. particles
14 would be appreciated.

15
16 We added the following sentences to the manuscript.

17 **The penetration of muons and electrons were simulated in GEANT4 simulation framework (Olah, L.**
18 **et al., 2019). The analysis cut on the goodness of track fit was set to 1.5 to suppress the penetration**
19 **of muons down to 10 % those had the energy of < 1 GeV. This simulation study showed that the**
20 **electromagnetic component did not create signal in the MMOS.**

21
22 (3) 223.224: could you provide the detector spatial and angular resolutions ?

23
24 226: the 8×8 mrad² angular binning corresponds to the angular resolution ? see also previous comment.
25 A mistyping is also reported in the technical corrections section.

26
27 We added the following sentences to the manuscript.

28 **The wire distances were designed to be 12 mm in MWPC detectors to provide a fair positional**
29 **resolution of approx. 4 mm even if lead plates were applied between the MWPCs (Varga, D. et al.,**
30 **2015; Varga, D. et al., 2016; Olah, L. et al., 2018). The angular resolution of 1.5 meter-length**
31 **tracking system was approx. 2.7 mrad (Olah, L. et al., 2018).**

32
33
34
35 (4) 254: Since the convex level of the mound is small [. . .] Could you clarify the meaning ?

37 We rephrased the text as follows.

38 Since the aspect ratio of the mound, i.e., the ratio of its width to its height (10:1) was large,

39

40 (5) 260: An indication of the total number of muons collected and of the contents of muons recorded in
41 the bins could be appreciated.

42

43 We added the following sentences to the manuscript.

44 The total number of muons collected at Position A in the elevational-angle-region
45 below 180 mrad was 76,682. The number of muons recorded in the bins at an azimuthal
46 angle of 0 ranged from 30 to 500, depending on the elevational angle.

47

48 The total number of muons collected at Position B in the elevational-angle-region below
49 180 mrad was 15,214. The number of muons recorded in the bins at an azimuthal angle
50 of 0 ranged from 15 to 100, depending on the elevational angle.

51

52 (6) 261: could you better describe what are the background and foreground mound and the effect on the
53 measurement ?

54

55 We rephrased the text as follows.

56 The bottom right green-colored region in Figure 3, where the number of muons was
57 counted less than other regions corresponds to the direction because in the positive
58 azimuthal angular region at Position A, the rectangular section of the mound provided
59 the additional path length for muons that arrived at lower elevation angles.

60

61 (7) 263: I think that it is not appropriate to claim here a lower density region since no normalization to the
62 effective thickness of material crossed by muons have been applied to the plot of Figure 3.

63

64 We removed the following sentences from Results section.

65

66 The reddish patch that can be seen on the left side of this green-colored region indicates a
67 low-density collapsed landslide mass on the northern slope of the mound.

68

69 Also, we removed the following related sentences from Discussion section.

70

71 (A) The reddish patches that can be seen on the left side of Images A and B indicate an existence of
72 a large-scaled collapsed landslide mass on the northern slope of the mound. The collapsed landslide

73 mass has a significant amount of the interparticle space; hence a lower density in comparison to the
74 surrounding regions.
75

76 The claim in Discussion section will not be affected by removing these sentences.
77

78 (8) 311: almost doubly defined density structure was imaged. It is not clear to me the sense. Please
79 describe better.
80

81 We rephrased the text as follows.
82 Since the distance to the mound peak (50 m) was closer at Position B, **the spatial resolution at the**
83 **mound peak was improved for a given angular resolution of the tracker.**
84

85 (9) 347: do you have an estimation of the percentage variation of the density ?
86

87 Related to the comment (7), since it was not appropriate to claim a lower density region
88 since no normalization to the effective thickness of material crossed by muons have
89 been applied to the plot of Figure 3, this part was removed from the manuscript.
90

91 (10) 226: 8x8 mrad -> 8 mrad x 8 mrad
92

93 Corrected.
94

95 (11) Figure 3: vertical axis unit is in rad and not in mrad.
96

97 Corrected.
98

99 Replies to Anonymous Referee #2
100

101 (1) Fig. 1 is a very relevant figure for the measurement environment, however it is too C1 GID Interactive
102 comment Printer-friendly version Discussion paper dense. E.g. 1.150 says Scalps A and B in Figure 1,
103 which is not identifiable to me.
104

105 “Scalps A and B” were removed from the sentence. Instead, we rephrased it to
106 “large-scale rotational landslide occurred in **the north side of the round-shaped section** of the burial
107 mound.” so that the reader can recognize them from Figure 1.
108

109 (2) Figure caption refers to "solid curves", which are probably with matching color with the viewing
110 directions (red and blue), but otherwise there are a lot of solid curves on the figure (e.g. landslides).

111

112 It may be a possibility to split the image into two, one more for the existing geometry, the other for the
113 interpretation (indicating Cracks / Scalps, observation direction elevations, etc). The int

114

115 We added an inset to Figure 1 so that the geometrical information is separately given
116 in the figure. The caption was modified so that the indication of the solid curves
117 could be more distinctive.

118

119 (3) It would be important to make the captions precisely matching with the figure (e.g. the image is now
120 gray below the explanatory lines and writing; on the left bottom caption "Landslides" are with gray
121 shaded area and black line. Figure has no black lines. (also later 1.266 says "scalps (arc-shaped lines in
122 Figure 1)".)

123

124 We modified the color of the arc-shaped lines and trench marks in the legend so that
125 they matched with the ones in the topographic drawings.

126

127 (4) 1.326 argues for significance "was overall more than 1 sigma", which is not too convincing. To me it
128 looks more like 2-3 sigmas, in multiple independent measurement points.

129

130 We added a phrase. "The statistical significance was overall more than 1σ , but was increased to $2-3\sigma$
131 in the shallower region of the mound."

132

133 (5) L.325 says "angle range between 264-424 mrad", which seems the combination of Crack A and B,
134 however, 1.327 says "associated with the same scalp (Scalp A). Please clarify.

135

136 We rephrased the sentence. "This low-density region was interpreted as the combination of
137 Cracks A and B"

138

139 (6) There seems a confusion on figure numbering, now there are two different Figure 3-s, probably the
140 colored muogram around 1.273 is Figure 3, and around 1.300 (Azimuthal distribution...) is Figure 4. On
141 this latter, indicate panels A, B and C. 1.323 refers to Figure 6, which is non-existent, but must be the
142 Figure 5. Please check carefully the figure numbering and its consistence in the text references.

143

144 Corrected.

145

146 (7) 1.20: "... recorded in this historical heritage sites." Here "sites" should be singular (heritage site).

147

148 Corrected.

149

150 (8) (Introduction: the word "however" is used a bit too often (1.31, 1.33, 1.40, 1.62), breaking the
151 argumentation line. Consider replacing some by re-wording, if seems appropriate)

152

153 The second however was replaced with other wording so that this word appears less
154 frequently.

155

156 (9) 1.148: Conversely, It was... ("it" should not be with capital)

157

158 Corrected.

159

160

161

162

163

164

165

166

167

168

169

170

171

172

173

174

175

176

177

178

179

180 Muography as a new tool to study the historic earthquakes
181 recorded in ancient burial mounds

182

183 Hiroyuki K.M. Tanaka^{1,2}, Kenji Sumiya³, László Oláh^{1,2}

184

185 ¹Earthquake Research Institute, The University of Tokyo, 1-1-1 Yayoi, Bunkyo, Tokyo
186 113-0032, Japan

187 ²International Muography Research Organization (MUOGRAPHIX), The University of
188 Tokyo, 1-1-1 Yayoi, Bunkyo, Tokyo 113-0032, Japan

189 ³Graduate School of Informatics, Kansai University, 2-1-1 Ryozenji-cho, Takatsuki-shi,
190 Osaka 569-1095, Japan

191

192

193 **Abstract**

194 Bidirectional muographic measurements were conducted at the Imashirozuka burial
195 mound, Japan. The mound was built in the beginning of the 6th century as a megalithic
196 tomb and was later collapsed after a landslide caused by the 1596 Fushimi Earthquake,
197 one of the largest earthquakes that have occurred in Japan over last few centuries. The
198 measurements were conducted in order to find evidence of this past disaster recorded in
199 this historical heritage **site**. As a result, the vertical low-density regions were found at
200 the top of the mound. These regions were interpreted as large-scale vertical cracks that
201 caused the translational collapse process behind the rotational landslide that was already
202 found in the prior trench-survey-based works. These results indicate that there was an
203 intrinsic problem with the stability of the basic foundation of the Imashirozuka mound
204 before the 1596 Fushimi Earthquake.

205

206

207 **1. Introduction**

208 By expanding our understanding of past large-scale natural disasters, such as tsunami,
209 earthquakes and volcanic eruptions, future hazards can be extrapolated and estimated.
210 However, modern scientific records of these natural disasters only, for the most part,
211 cover events from the last couple of centuries, which have been recorded by scientific
212 instruments only in limited regions throughout the world. On the other hand,

213 geographical or topographical modifications are often physically recorded in the land
214 surface as a result of such large-scale natural disasters, and correct methodologies can
215 be deciphered to infer unknown details about these events. For example, a large-scale
216 volcanic eruption usually creates a large volume pyroclastic flow, which later remains
217 in the geological stratum as a sedimentation of volcanic products. By applying a
218 geological dating technique to these past remnants of the eruptions, we can infer the
219 timing and the magnitude of the past disasters. However, the geological timescale is
220 largely different from that of human history, and the dating precision by these
221 geochronological techniques is limited to an order of 100 years. On the other hand,
222 historical studies often provide records that can be verified with yearly or sometimes,
223 daily precision, depending on how far back the disaster occurred. Historical information
224 is more straightforward regarding affected sites and the year or date of the disaster. For
225 example, this information can come from literature, which describes destruction by
226 earthquakes or repairs after earthquakes, providing valuable evidence for the location of
227 earthquakes and the effects brought by these earthquakes. Therefore, if we can combine
228 the historian's knowledge with the analysis results of these past disaster remnants,
229 historical records become valuable information which can help to improve the accuracy
230 of these geological dating techniques by developing into an iteration process. The
231 derivation by scientists and engineers have been utilized as evidence of earthquakes and
232 which are later incorporated by historian to evaluate the dates of the events, and vice
233 versa.

234

235 Thus far, a combination of geological techniques and historical data have been applied
236 to historically well-studied objects to fill the gaps in our understanding of the historical
237 natural disaster record including tsunami (Daly et al., 2019; Dey et al. 2014),
238 earthquakes (Korjenkov and Mazor, 2003; Guidoboni et al., 1994; Ambraseys et al.
239 1983) and volcanic eruptions (Elson and Ort, 2018). The data are exploited mostly by
240 direct excavation of the historic site, and such anatomical techniques (similar in
241 principle to dissecting bodies to directly view organs within human bodies) allow us to
242 exploit regional, direct and detailed information; however, not all historical heritage
243 sites can be accessible and modified in this way. For example, due to the cultural
244 restriction, it is not always possible to conduct a trench survey to excavate the extant
245 historical structures such as the ancient monuments or public buildings to obtain the
246 geological knowledge about the past disaster remnants. Even when such a style of
247 investigation is approved, the exploitable information is usually localized. Thus, there is
248 a need for a non-invasive technique such as surface wave exploration, which would be

249 conducted to provide a more overall picture of targeted structures to increase the
250 possibilities of finding more physical evidence of past disasters.

251

252 Muography is a technique enabling us to "x-ray" gigantic (hectometric to kilometric)
253 objects. The surface of the Earth is constantly bombarded with muons, particles that
254 have decayed from cosmic rays arriving at the atmosphere from outside our solar
255 system, and these particles can be utilized as probes for muography. After traversing
256 targeted object, remnant muons are tracked with a particle detector located at lower
257 elevations than the region of interest inside the target. The result is a pattern of the
258 contrast in the density distribution inside the objects, which is projected on a
259 2-dimensional plane. Muography has been applied to image the internal structure of
260 volcanoes (Tanaka et al. 2007; Tanaka et al., 2009; Lesparre et al., 2012; Tanaka et al.,
261 2014; Olah et al., 2019), cultural heritages including Giza pyramids (Cheops and
262 Chephren), Egypt, Prambanan temples, Indonesia, Mt Echia, Italy and Santa Maria del
263 Fiore, Italy (Alvarez et al., 1970; Hanazato and Tanaka, 2016; Tanaka and Ohshiro,
264 2016; Morishima et al., 2017; Guardincerri et al. 2018; Cimmino et al. 2019), industrial
265 plants (Tanaka, 2013), and other natural (Tanaka et al., 2011; Olah et al. 2012; Schouten,
266 2018) and man-made structures (Mahon et al. 2018). Prior works have focused on
267 searching undiscovered chambers or the total weight of the heritage. Instead, in this
268 work, we applied muography to study ancient earthquakes for the first time. We focused
269 on the 1596 Fushimi Earthquake, one of the largest earthquakes that have occurred in
270 Japan over last few centuries and examine whether the technique of muography can
271 increase the possibilities of finding more physical evidence of past disasters recorded in
272 historical heritage sites.

273

274 **2. Observation**

275 Imashirozuka, an imperial burial mound in Japan was chosen as a target of the current
276 study. In Japan, imperial burial mounds have been well studied and a lot of knowledge
277 has accumulated. For the current study, this type of the burial mound has the following
278 advantages to study past earthquakes (Kamai et al., 2008). (A) The construction method
279 of the imperial mound is well studied by historians and thus, even if the mound has been
280 damaged by the past earthquakes, the original structure of the mound can be estimated.
281 (B) The imperial mound was built as a stable object, and thus collapsed areas inside the
282 mound would be likely to be records of past major earthquakes. (C) The imperial
283 mounds are in general situated in the urban area. Therefore, the collapsed mounds can
284 be used as an index to measure the past seismic disasters in urban areas long ago. (D) In

285 the recent human's history, various kinds of embankments have been built, but its
286 stability is discussed within the time scale of decades. The collapsed mounds offer us a
287 unique opportunity of geotechnical discussions within a time scale of centuries. (E) The
288 construction method of the mound was already well established when they were built.
289 The mounds built in the same era used the same construction method and thus it is
290 expected that the mechanical strength is the same. Therefore, the different collapsing
291 conditions among different mounds located near each other could infer different ground
292 conditions or different underwater conditions.

293

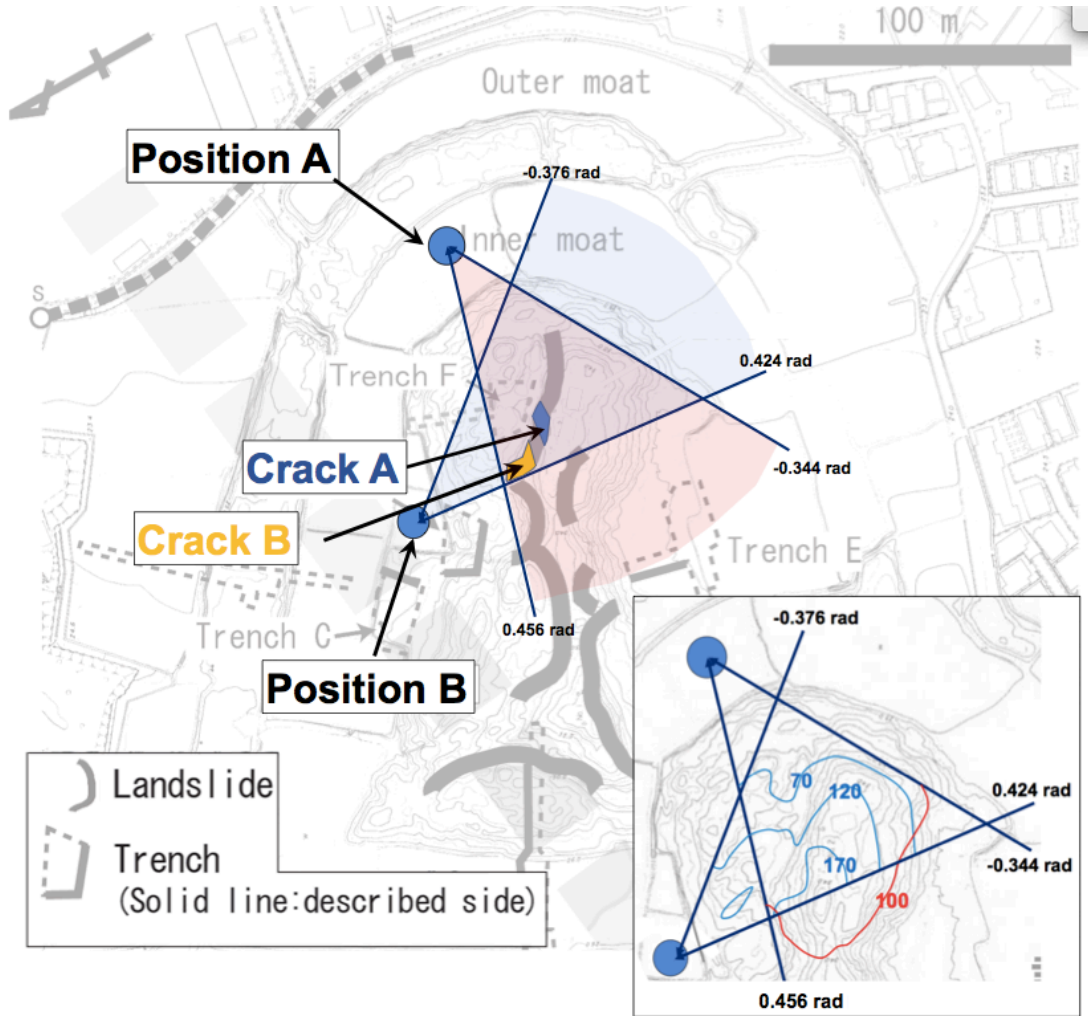
294 Imashirozuka is a keyhole-shaped imperial burial mound that was built in the beginning
295 of the 6th century in Japan. This burial mound is situated on one of the most active
296 faults in Japan, which is part of the Rokkou active fault system. This fault system
297 caused the Great Hanshin Earthquake in 1995. In 1596, it is thought that this Rokkou
298 active fault system and the next neighbor fault system called the Arima-Takatsuki
299 tectonic line were activated at the same time, and one of the largest earthquakes in the
300 last few centuries, Fushimi Earthquake, (Magnitude 7.25-7.75) occurred (Kamai et al.,
301 2008). The total length of the Imashirozuka mound is 190 m and the height is 11-12 m.
302 Although this burial mound was originally built in the triple-layered structure, the top
303 layer collapsed after a landslide. The collapse occurred more extensively in the northern
304 part of the mound. The level of damage depends, in general, on the ground motion
305 during an earthquake, which itself depends on its magnitude and distance from the site.
306 This extensive collapse is probably due to the existence of the Ai fault line, a part of the
307 Rokkou active fault system, is located closer to the northern part of the mound.
308 Currently, Imashirozuka mound consists of a base layer made of high bulk density
309 sandy clay (a soil particle density of 2.6 gcm^{-3} with a porosity of 52%), and a middle
310 layer made of lower bulk density granules (a soil particle density of $2.6\text{-}2.8 \text{ gcm}^{-3}$ with a
311 porosity of 76%) (Kamai et al., 2008). The s-velocity structure observed in the base
312 layer was faster (harder) in comparison to the middle layer (Kamai et al., 2008). For
313 the purpose of the archaeological studies, 6 trenches were excavated and landslide
314 remnants were observed in many of these trenches. The burial mound was originally
315 surrounded by a double moat, but most of this moat was buried in the past, and only a
316 part of it currently remains. The landslide deposits originated from the sediments in the
317 moat were dated, and the results were 1420-1510 AD with a method of the C^{14} dating
318 (Sangawa and Miyazaki 2001). Since it is known that Fushimi Earthquake occurred in
319 1596, this burial mound collapse was thought to have been triggered by this earthquake
320 (Sangawa and Miyazaki 2001).

321

322 The top view of the landslides generated by the 1596 Fushimi Earthquake is shown in
323 Figure 1 (Kamai et al., 2008). The results of the trench survey indicated that most of the
324 landslide types were represented by a combination of translational and rotational
325 landslides (Kamai et al., 2008). Movement was inferred with the following sequence: 1.
326 the landslide mass moved near horizontally for a few meters, 2. the transported
327 landslide mass reached the inner moat, 3. the landslide mass slid down and shifted from
328 translational to rotational landslide mode. Conversely, it was found that an
329 exceptionally large-scale rotational landslide occurred in the north side of the
330 round-shaped section of the burial mound. Whether the burial mound deformation
331 related to this rotational slide is connected to the translational landslide had continued to
332 be a mystery. The purpose of this work was to examine whether muographically found
333 evidence can be used to address this question.

334

335



336

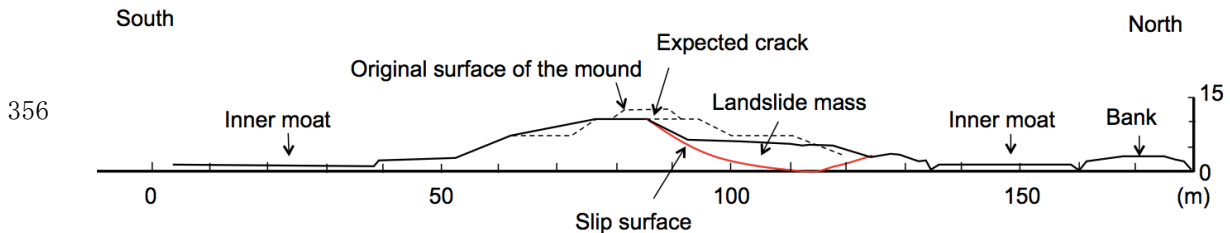
337 Figure 1. Top view of Imashirozuka burial mound. Positions A and B indicate the
 338 locations of the detectors for the current bidirectional muographic observations. The
 339 shaded areas in red and blue indicate the viewing angle of each measurement. **The inset**
 340 **shows the geometrical information of the mound. The red and blue solid curves**
 341 **respectively indicate the cross sections of the mound at given elevation angles from**
 342 **Positions A and B. The red and blue numbers indicate the elevation angles in units of**
 343 **mrاد.**

344

345 In Figure 2, the cross-sectional view of the mound sliced along Line F in Figure 1 is
 346 shown. This structure has been modeled based on the trench surveys conducted in 2008
 347 (Kamai et al. 2008). Original surface of the mound (dashed lines in Figure 2) that was
 348 estimated from the past archaeological studies, was lost by the landslide triggered by the
 349 1596 Fushimi earthquake. The red lines indicate the slip surface of the landslide and at
 350 the top of this surface, the existence of near-vertical cracks was expected. From these

351 trench surveys, the region indicated between the red lines and the solid black lines in
352 this figure was interpreted as the landslide mass, and displayed lower density than the
353 other part of the mound and thus, it was expected that muons could penetrate more in
354 this region (in particular at the top of this region).

355



357 Figure 2. Cross-sectional view of the mound along Line F in Figure 1. The dashed lines
358 indicate the original surface of the mound, and the red lines indicate the slip surface of
359 the landslide triggered by the 1596 Fushimi earthquake. The authors drew this image
360 based on the work done by Kamai et al. (2008).

361

362 Mechanical fractures within rock and soil produce a significant amount of interparticle
363 space and these fractured zones are detected as lower-density-regions in muographic
364 images (Tanaka and Muraoka, 2013, Carbone et al. 2014). Likewise, when a landslide
365 occurs, various processes influence changes in the density distribution inside a burial
366 mound. When a crack is generated in the burial mound, the density is reduced along the
367 crack. If a large-scale collapse occurs, the collapsed landslide mass will contain a lot of
368 inter-particle voids, and the density will be reduced. If the geometrical arrangement is
369 altered between the high-density base layer and lower density middle layer due to the
370 ground motion such as a fault slip, the overall density distribution will be altered
371 accordingly. All of these variations can be imaged with muography.

372

373 **3. Method**

374 Bidirectional muographic measurements were conducted at the Imashirozuka burial
375 mound site so that the resultant images could be used for 3-dimensional interpretation of
376 the internal structure of the circular section of the mound. In particular, one of the
377 detector positions of the current bidirectional measurements were chosen on the
378 northern side of the round-shaped section (Position B) so that the area where the
379 extensive collapse occurred could be more closely observed. The positions chosen for
380 the current measurement are shown in Figure 1. The first measurement of the
381 Imashirozuka mound started at Position A on September 21, 2019. The data were taken
382 for 40 days, and subsequently the detector was moved to Position B to collect the data

383 for another period of approximately one month.

384

385 The detector employed for the current measurement was the multi-wire proportional
386 chambers (MWPC) based muographic observation system (MMOS) that consists of 6
387 layers of MWPCs and lead plates with a total thickness of 10 cm. A detailed description
388 of the MMOS can be found in elsewhere (Olah et al. 2018), and thus only the main
389 features are briefly introduced here. In between each of the MWPC, a 2-cm thick lead
390 plate accommodated in a 4 mm-thick-stainless steel case is inserted, thus the total
391 thickness of these radiation shields is equivalent to $\sim 130 \text{ gcm}^{-2}$. These radiation
392 shields function as an absorber or a scatterer of low energy background particles that
393 include muons or other electromagnetic particles. **The wire distances were designed to**
394 **be 12 mm in MWPC detectors to provide a fair positional resolution of approx. 4 mm**
395 **even if lead plates were applied between the MWPCs (Varga, D. et al., 2015; Varga, D.**
396 **et al., 2016; Olah, L. et al., 2018). The angular resolution of 1.5 meter-length tracking**
397 **system was approx. 2.7 mrad (Olah, L. et al., 2018). Only the straight trajectories**
398 **throughout 6 detectors are employed and recorded as muons. The penetration of muons**
399 **and electrons were simulated in GEANT4 simulation framework (Olah, L. et al., 2019).**
400 **The analysis cut on the goodness of track fit was set to 1.5 to suppress the penetration of**
401 **muons down to 10 % those had the energy of $< 1 \text{ GeV}$. This simulation study showed**
402 **that the electromagnetic component did not create signal in the MMOS.** In the current
403 measurements, the total weight of the MMOS was 600 kg including the case, batteries
404 and gas bottle. The total power consumption of the detector was $\sim 30\text{W}$, and the six
405 400-Wh lithium-ion batteries loaded into the case allowed us the continuous operation
406 for 80 hours, and the recurrent charging and replacements of the batteries further
407 extended the time of the continuous operation. The flow rate of the Ar-CO₂ gas mixture
408 (Ar:80, CO₂:20) through the chambers was 1–2 liters per hour to enable continuous
409 operation for a few months with a standard 40L type (6,000 liters) gas bottle. The
410 casters attached to the bottom of the case facilitated movements of the detector around
411 the mound. Moisture absorbent boxes were equipped inside the box in order to retain
412 the humidity at a constant level around the MWPCs. The size of the active area of the
413 detector was $80 \times 80 \text{ cm}^2$, and the distance between the uppermost and lowermost
414 stream detectors were 150 cm. The recorded muon tracks were stored and the numbers
415 of muon counts were directionally sorted out into a matrix with an angular binning
416 width of $8 \text{ mrad} \times 8 \text{ mrad}$. As is indicated in Figure 1, the azimuthal viewing angle was
417 $\pm 500 \text{ mrad}$, however, due to the smaller geometrical acceptance for larger angles, only
418 the data within $\pm 400 \text{ mrad}$ were used. The detector cost was $\sim 60\text{k}$ US dollars, but the

419 operational cost was suppressed to a few thousand US dollars for entire operation
420 including the transportation, human resources for battery replacements and data
421 download.

422

423 Since the current target size is an order of 100 m, the following simplified analytical
424 expression can be applied for derivation of the relative density variations inside the
425 target volume because the muon's cutoff energy (the minimum energy of the muons that
426 can escape from the target volume) is much lower than the critical energy, 708 GeV in
427 SiO₂, the continuous ionization process is the main energy loss process (Tanaka and
428 Ohshiro, 2016).

429

$$430 \quad I_0/I_1=(X_0/X_1)^{-\gamma}, \quad (1)$$

431

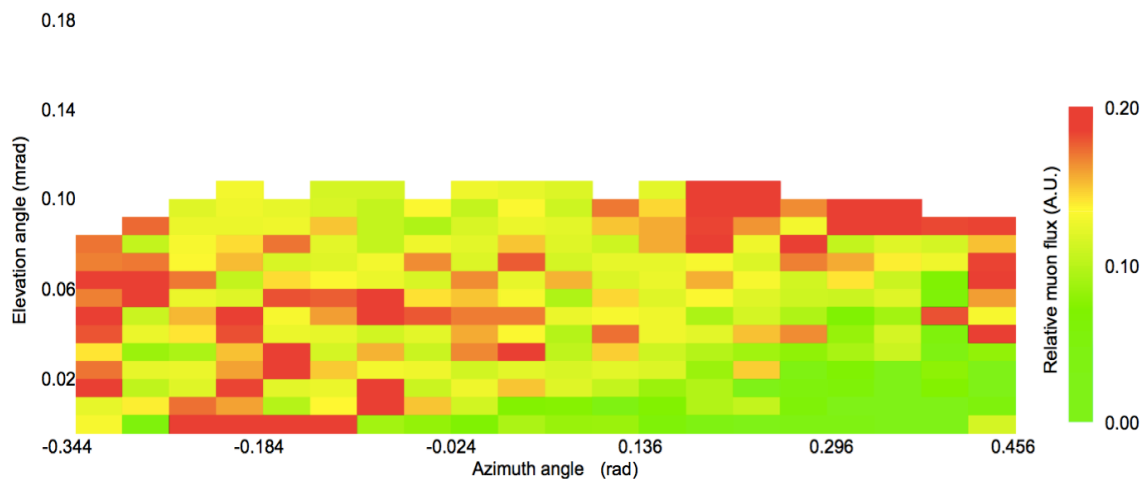
432 where I_0 and I_1 is the remnant muon flux after passing through different densimetric
433 thickness of rock X_0 and X_1 . The Greek symbol, γ , is the zenith-angular dependent index
434 of the power law of the integrated muon spectrum within 50-200 GeV. In this work,
435 only the “relative muon flux” was used for discussions of the density contrast inside the
436 mound. The obtained matrix has been normalized by the azimuthal distribution of the
437 open-sky flux so that the azimuthally angle-dependent acceptance has been canceled in
438 the image.

439

440 **4. Results**

441 Figure 3 shows the muographic image (Image A) taken at Position A that is indicated in
442 Figure 1. Corresponding azimuthal angles (-0.344 rad - 0.456 rad) are shown in Figure 1.
443 The distance between the detector and the peak of the mound was 70 m, and thus the
444 elevation angle of the mound peak was ~110 mrad (~6 degrees). Since **the aspect ratio**
445 **of the mound, i.e., the ratio of its width to its height (10:1) was large**, the matrix was not
446 re-binned in the elevational direction, but was re-binned in 40 mrad in the azimuthal
447 direction in order to increase the statistics. **The total number of muons collected at**
448 **Position A in the elevational-angle-region below 180 mrad was 76,682. The number of**
449 **muons recorded in the bins at an azimuthal angle of 0 ranged from 30 to 500, depending**
450 **on the elevational angle**. The data were normalized to the azimuthal distribution of the
451 open-sky muon tracks that was unaffected by the existence of the mound, which
452 corresponds to the elevational region between 300 and 360 mrad in order to derive the
453 “relative muon flux”. The bottom right green-colored region in Figure 3, where the

454 number of muons was counted less than other regions corresponds to the direction
 455 because in the positive azimuthal angular region at Position A, the rectangular section
 456 of the mound provided the additional path length for muons that arrived at lower
 457 elevation angles. It was expected that the region around landslide headscarps
 458 (arc-shaped lines in Figure 1) had cracks, and thus the average density along these
 459 cracks was significantly lower than the density around these. This density reduction
 460 effect is maximized in muographs when the muon's ray path is parallel to these cracks.
 461 From Position A, this direction corresponds to the azimuthal angular range between 200
 462 mrad and 300 mrad (see the position indicated by "Crack A" in Figure 1).
 463

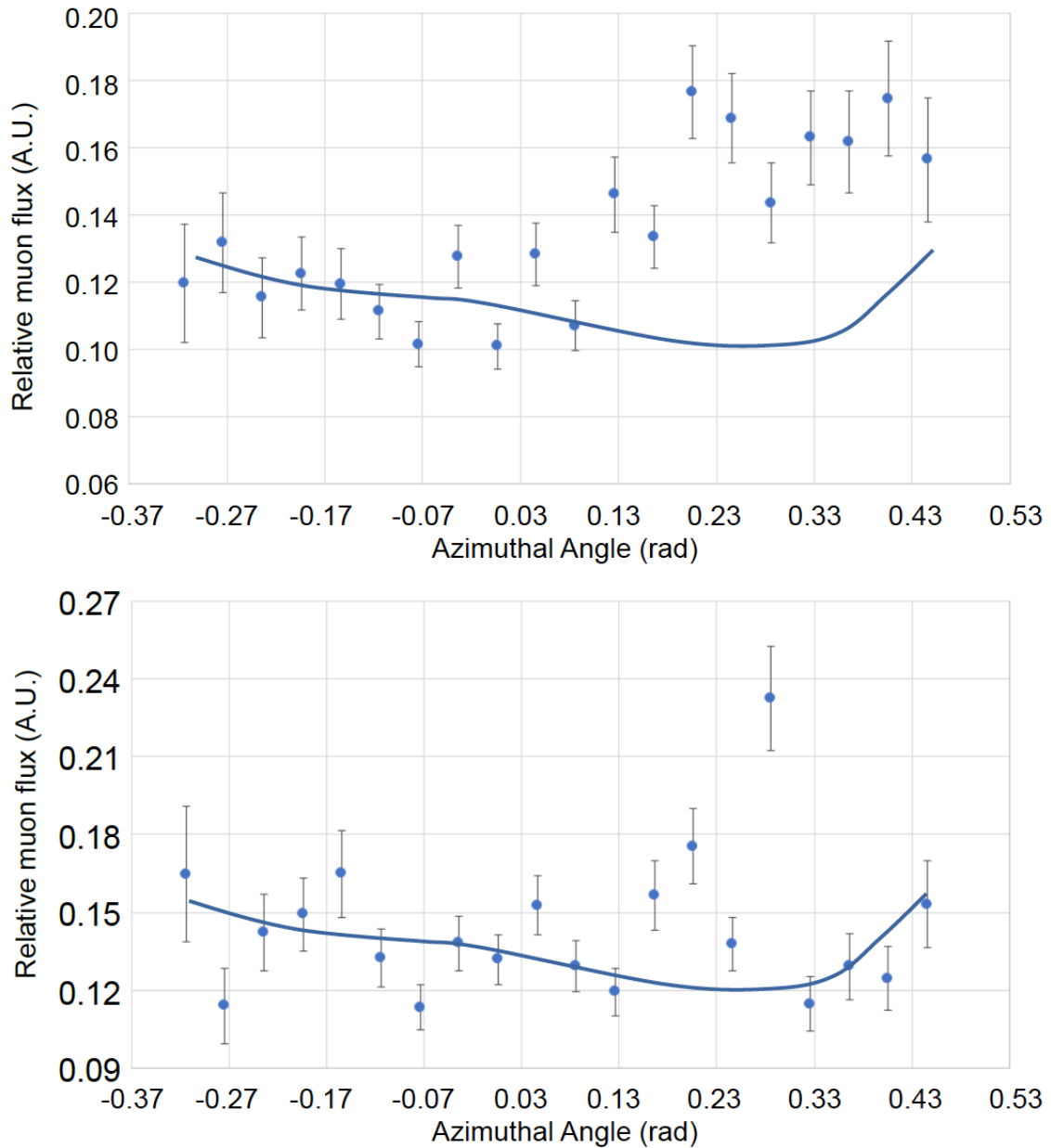


464
 465 Figure 3. Angular distribution of the relative muon flux, as was observed from the
 466 measurement at Position A. The horizontal and vertical bin widths are respectively 40
 467 mrad and 8 mrad. The azimuthal distribution of the relative muon flux was normalized
 468 to the total number of muons counted at each elevation angle.

469
 470
 471 Figure 4 shows the azimuthal distribution of the relative muon flux at shallow depths (at
 472 elevation angles of 108 mrad (Figure 4A) and 100 mrad (Figure 4B)). The solid lines
 473 are the expected muon flux. These lines were drawn based on the geometrical thickness
 474 of the mound along the muon paths (Figure 1) by assuming the uniform density
 475 distribution inside the mound. In these three images, the following three features can be
 476 found. (A) Overall, the excessive flux of muons was observed in the positive azimuthal
 477 angle region. This indicates that the average density in the positive azimuthal angle
 478 region is lower than that in the negative angle region. An overall density variation
 479 between them is 10-20%. (B) A strongly excessive muon flux can be found in the

480 azimuthal angle region between 176 mrad and 296 mrad in Figures 4A and 4B. The
481 statistical significance was more than 4σ . (C) In Figures 4A, there is also a low-density
482 region within the azimuthal angle range between 296-456 mrad. The position of this
483 low-density region corresponds to that of Trench F (dotted lines in Figure 1). From (A)
484 and (B), it was inferred that a large almost vertical crack exists in the shallow region,
485 however its existence was not clear when it's deeper than 2 m because of the effect of
486 overlapping the rectangular-shaped background mound (see the green-colored area at
487 the right bottom region of Figure 3). The density variations of this possible crack were
488 20-30% in comparison to the average density of the other part of the mound. The crack
489 width was 80-120 mrad that was equivalent to 6-8 m when considering the distance
490 between the detector and Crack A of 70 m.

491



492

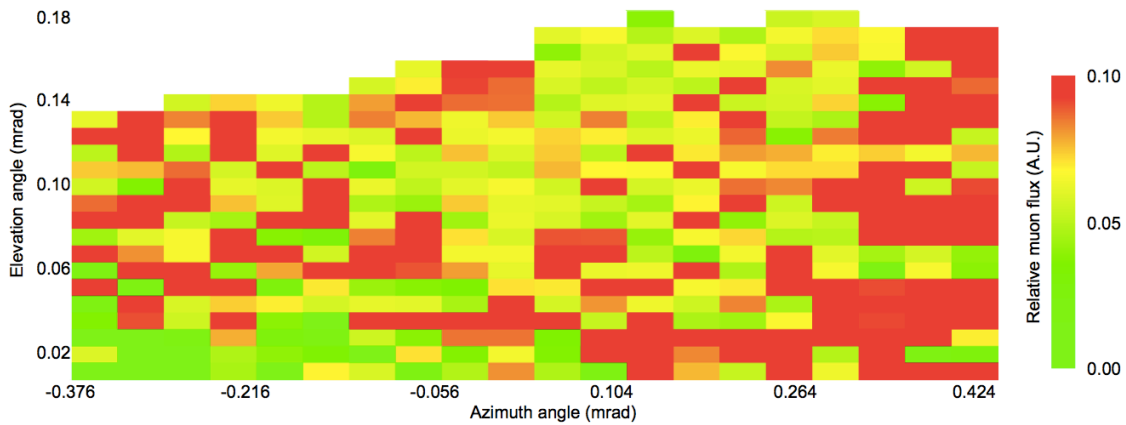
493 Figure 4. Azimuthal distribution of the relative muon flux for elevation angles of 100
 494 mrad (top) and 92 mrad (bottom). The solid curves indicate the expected horizontal
 495 muon flux variations.

496

497

498 Crack A was not parallel to the muon's ray path at Position B (Figure 1), however,
 499 Crack B was parallel to those in the azimuthal angle range between 300-420 mrad.
 500 Therefore, it was expected that the similar structure to Crack A would be observed in
 501 this angular region. Figure 5 shows the muographic image (Image B) taken at

502 Position B. Since the distance to the mound peak (50 m) was closer at Position B, the
 503 spatial resolution at the mound peak was improved for a given angular resolution of the
 504 tracker. The total number of muons collected at Position B in the
 505 elevational-angle-region below 180 mrad was 15,214. The number of muons recorded
 506 in the bins at an azimuthal angle of 0 ranged from 15 to 100, depending on the
 507 elevational angle. The data were normalized to the azimuthal distribution of the muon
 508 tracks recorded within the elevational range between 300 and 360 mrad in order to
 509 derive the “relative muon flux”. Corresponding azimuthal angles (-0.376 rad - 0.424
 510 rad) are shown in Figure 1.
 511

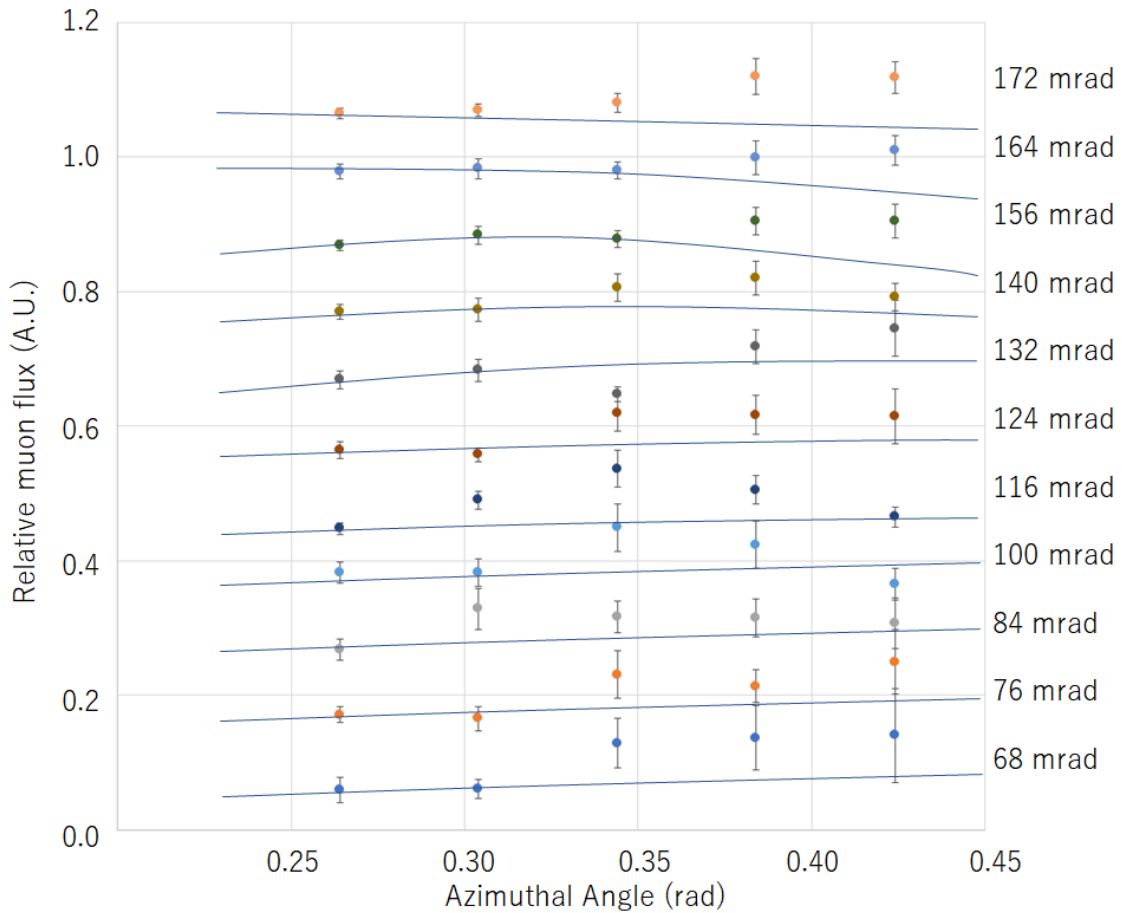


512
 513 Figure 5. Angular distribution of the relative muon flux observed at Position B. The
 514 horizontal and vertical bin widths are respectively 40 mrad and 8 mrad. The azimuthal
 515 distribution of the relative muon flux was normalized to the total number of muons
 516 counted at each elevation angle.

517
 518
 519 In Figure 6, the azimuthal distribution of the relative muon flux for elevation angles of
 520 68 mrad - 172 mrad are shown. In these images, the excessive muon flux was found
 521 within the azimuthal angle range between 264-424 mrad. The statistical significance
 522 was overall more than 1σ , but was increased to $2-3\sigma$ in the shallower region of the
 523 mound. This low-density region was interpreted as the combination of Cracks A and B,
 524 and it was found that the vertical extent of the crack was much deeper than what could
 525 be seen in Image A. The crack width was at least 80-160 mrad that was equivalent to
 526 4-8 m when considering the distance between the detector and Crack B. The reddish
 527 region in Figure 5 that can be seen on the left side of Crack B indicates low-density

528 collapsed landslide mass, with a mixture of the remnant of the past excavation at Trench
529 F.

530
531



532

533 Figure 6 Azimuthal distribution of the relative muon flux for various elevation angles.
534 The solid curves indicate the expected horizontal muon flux variations. The relative
535 muon flux values were multiplied for better visualization.

536

537

538

539 **5. Discussion**

540 From the bidirectional muographic images taken in the current measurements, the
541 following interpretations were derived.

542

543 The vertical low-density regions at the top of the mound in Images A and B show that
544 there is a large-scale vertical crack behind Landslide headscarp. The widths of these

545 vertical cracks were both 4-8 m thus it is reasonable to assume they are associated with
546 the same scarp.

547

548 In conclusion, the following picture was proposed. In prior trench-survey-based works,
549 most of the landslides that deformed this burial mound structure were found to have
550 been caused by a translational process. On the other hand, there was an exceptionally
551 large-scale rotational slide was found in the north region of the round-shaped section of
552 the mound, and the stone chamber was deformed and destroyed by this collapse process.
553 However, in the current muographic observations, a large-scale vertical crack was
554 discovered at the top of the round-shaped section, and it was found that the burial
555 mound deformation that connected to the translational collapse process also occurred
556 behind this rotational landslide. These data indicate that there was an intrinsic problem
557 with the stability of the basic foundation of the Imashirozuka mound before the 1596
558 Fushimi Earthquake. Changes in the foundation as a response to shaking from the
559 earthquake may have produced this large-scale burial mound collapse.

560

561 The burial mound seems to have a robust structure, more stable against earthquakes
562 than slender buildings like clock towers. However, a number of the ancient burial
563 mounds throughout Japan have collapsed from earthquakes and many modern buildings
564 are now built upon them. A small fraction has survived since early times, however, they
565 do not always indicate the earthquake-free sites. They represent an example of the final
566 designs of ancient Japanese construction since they have remained even after having
567 experienced a number of destructive earthquakes.

568

569 The technique of muography, which can probe seismically damaged ancient mounds is
570 similar to medical radiography which seeks to find the position, formation, and size of
571 the fractured zone inside the human body. In general, it is difficult to understand the
572 extent of damage, for example, of a patient's external wound without also understand
573 what is happening inside the body. The outside structure of ancient mounds is similar.
574 The surface of them has usually been naturally or artificially eroded with added
575 vegetation covering the shape during a long period of time it has existed. However, the
576 inside is more intact. For this reason, the trench survey technique (physically digging a
577 trench into the structure) to understand the "inside" can reveal valuable data.
578 However, similar to the manner in which x-ray photographs are usually applied to a
579 diagnosis before surgery is considered, muography is a more convenient and
580 noninvasive technique to effectively understand the overall inside structure to assess the

581 effect of time and natural disasters on the structure as a whole.

582

583 The current proof of concept measurement has attempted to show whether the technique
584 of muography increases the possibilities of finding more physical evidence related to
585 past earthquakes by selecting the Imashirozuka mound as an example. Obviously, the
586 specific earthquake damage of each burial mound is unique and cannot be generalized.
587 Its response depends not only on its material properties of the mound including its
588 mechanical properties of its foundations (strength and rigidity), but also on the ground
589 motion during an earthquake. Surveying and mapping various mounds that are thought
590 to be affected by the earthquake will provide a valuable data for us to verify and sort out
591 the factors that caused the damage.

592

593 Not only Imashirozuka mound but also other various burial mounds including the
594 Mishima mound group and the Kobo mound group are concentrated along the Rokkou
595 active fault system and its next neighbor Arima-Takatsuki tectonic line. The current
596 muographic results suggest that a combination of muography and the techniques of
597 trench survey or other conventional geophysical techniques can contribute towards the
598 construction of a more comprehensive understanding of the seismic response and
599 deformation of each burial mound. The characteristics of muography would allow
600 researchers to conduct an investigation of several sites quickly and efficiently to grasp
601 the general trend of the ensemble of these sites. Incorporating the muography
602 visualization technique into engineering expertise and in conjunction with historical
603 comparanda would utilize a new potential: by acquiring this new, valuable data from
604 these ancient burial mounds in Japan and other similar sites worldwide, we would
605 increase our ability to tackle future challenges of natural disaster preparation.

606

607 **Acknowledgements**

608 The authors acknowledge Toshitaka Kamai for valuable discussions about the current
609 muographic observation results. The authors also acknowledge Takefumi Hayashi for
610 his coordination and support the current measurements, Fumitaka Yoneda & Chikara
611 Inoue for their valuable archaeological advice, Ichiro Kanegae for provision of past
612 excavation research materials of Imashirozuka mound, and Masao Uchida for his
613 support as a chief administrator of Imashirozuka park. The authors acknowledge two
614 anonymous referees for their valuable suggestions.

615

616 **References**

617 Alvarez, L. W., Anderson, J. A., El Bedwei, F., Burkhard, J., Fakhry, A., Girgis, A.,
618 Goneid, A., Hassan, F., Iverson, D., Lynch, G., Miligy, Z., Moussa, A. H., Sharkawi, A.,
619 and Yazolino, L.: Search for hidden chambers in the pyramid, *Science*, 167, 832– 739,
620 doi:10.1126/science.167.3919.832, 1970.

621

622 Ambraseys NN., Banda E., Irving J., Mallard D., Melville C., Morse T., Muir-Wood R.,
623 Munoz D., Serva L., Shilston D., Surinach E., Vogt J.: Notes on Historical Seismicity.
624 *Bull. Seismol. Soc. Am.* 73(6), 1917–1920, 1983.

625

626 Carbone, D., Gibert, D., Marteau, J., Diament, M., Zuccarello, L., and Galichet, E.: An
627 experiment of muon radiography at Mt. Etna (Italy), *Geophys. J. Int.*, 196, 633–643,
628 2013.

629

630 Cimmino, L., Baccani, G., Noli, P., Amato L., Ambrosino, F., Bonechi, L., Bongi, M.,
631 Ciulli, V., D’Alessandro, R., D’Errico, M., Gonzi, S., Melon, B., Minin, G., Saracino,
632 G., Scognamiglio, L., Strolin P., Viliani, L.: 3D Muography for the Search of Hidden
633 Cavities, *Scientific Reports* 9, 2974, 2019.

634

635 Daly, P., Sieh, K., Yew Seng, T., McKinnon, EE., Parnell, AC., Ardiansyah, R., Feener,
636 M., Ismail, N., Nizamuddin, Majewski J.: Archaeological evidence that a late
637 14th-century tsunami devastated the coast of northern Sumatra and redirected history,
638 *PNAS*, 116 (24) 11679-11686, 2019

639

640 Dey, H., Goodman-Tchernov, B., Sharvit, J.: Archaeological evidence for the tsunami
641 of January 18, A.D. 749: a chapter in the history of Early Islamic Qaysariyah (Caesarea
642 Maritima), *Journal of Roman Archaeology*, 27, 357-373, 2014.

643

644 Elson, M., Ort, M.H.: *Archaeological Volcanology*, *The Encyclopedia of*
645 *Archaeological Sciences*. Edited by Sandra L. López Varela. John Wiley & Sons, Inc.,
646 1-5, 2018.

647

648 Guardincerri E., Bacon JD., Barros N., Blasi C., Bonechi L., Chen A., D’Alessandro R.,
649 Durham JM., Fine M., Mauger C., Mayers G., Morris C., Newcomer FM., Okasinski J.,
650 Pizzico T., Plaud-Ramos K., Poulson DC., Reilly MB., Roberts A., Saeid T., Vaccaro
651 V., Van Berg R.: Imaging the dome of Santa Maria del Fiore using cosmic rays, *Philos.*
652 *Trans. A Math. Phys. Eng. Sci.* 377 (2137) 20180136, 2018. doi:

653 10.1098/rsta.2018.0136.

654

655 Guidoboni, E., Comastri, A., Traina G., Catalogue of Ancient Earthquakes in the
656 Mediterranean Area up to the 10th Century, Istituto Nazionale di Geofisica, Rome,
657 1994.

658

659 Hanazato, T., Tanaka, HKM.: Inspection of the internal structure of the
660 UNESCO-World Heritage with cosmic rays, *Isotope News*, 741, 60-64, 2016.

661

662 Kamai, T., Sangawa, A., Shuzui, H.: Landslides on Ancient Burial Mounds Induced by
663 the 1596 Keicho-Fushimi Earthquake, *Jour. Japan Soc, Eng. Geol.*, 48, 6, 285-298,
664 2008.

665

666 Korjenkov, AM., Mazor E.: Archaeoseismology in Mamshit, Southern Israel, cracking a
667 millennia-old code of earthquake preserved in ancient ruins, *Archäologischer Anzeiger*,
668 2, 51-82, 2003.

669

670 Lesparre, N., Gibert, D., Marteau, J., Komorowski, J.-C., Nicollin, F., and Coutant, O.:
671 Density muon radiography of La Soufriere of Guadeloupe volcano: comparison with
672 geological, electrical resistivity and gravity data, *Geophys. J. Int.*, 190, 1008–1019,
673 2012.

674

675 Mahon D., Clarkson A., Gardner S., Ireland D., Jebali R., Kaiser R., Ryan M., Shearer
676 C., Yang G.: First-of-a-kind muography for nuclear waste characterization, *Philos.*
677 *Trans. A Math. Phys. Eng. Sci.* 377 (2137) 20180048, 2018. doi:
678 10.1098/rsta.2018.0048.

679

680 Morishima K., Kuno M., Nishio A., Kitagawa N., Manabe Y., Moto M., Takasaki F.,
681 Fujii H., Satoh K., Kodama H., Hayashi K., Odaka S., Procureur S., Attié D., Bouteille
682 S., Calvet D., Filosa C., Magnier P., Mandjavidze I., Riallot M., Marini B., Gable P.,
683 Date Y., Sugiura M., Elshayeb Y., Elnady T., Ezzy M., Guerriero E., Steiger V.,
684 Serikoff N., Mouret JB., Charlès B., Helal H., Tayoubi M.: Discovery of a big void in
685 Khufu's Pyramid by observation of cosmic-ray muons, *Nature*, 552(7685), 386-390,
686 2017. doi: 10.1038/nature24647

687

688 Olah L., Tanaka, HKM., Ohminato T., Hamar G., Varga D.: Plug Formation Imaged

689 Beneath the Active Craters of Sakurajima Volcano With Muography, *Geophys. Res.*
690 *Lett.*, GL084784, 2019. doi.org/10.1029/2019GL084784.

691

692 Olah, L., Barnaföldi, G. G., Hamar, G., Melegh, H. G., Surányi, G., and Varga, D.:
693 CCC-based muon telescope for examination of natural caves, *Geosci. Instrum. Method.*
694 *Data Syst.*, 1, 229–234, doi:10.5194/gi-1-229-2012, 2012.

695

696 Olah L., Tanaka HKM., Ohminato T., Varga D.: High-definition and low-noise
697 muography of the Sakurajima volcano with gaseous tracking detectors, *Sci Rep.* 8(1),
698 3207, doi: 10.1038/s41598-018-21423-9, 2018.

699

700 Sangawa, A., Miyazaki, Y.: Traces of Landslides found in Imashirosuka mound, 18th
701 meeting of Japan Society for Scientific Studies on Cultural Property, 24-25, 2001.

702

703 Schouten, D.: Muon geotomography: selected case studies, *Philos. Trans. A Math. Phys.*
704 *Eng. Sci.* 377 (2137) 20180061, doi: 10.1098/rsta.2018.0061, 2018.

705

706 Tanaka, H. K. M., Nakano, T., Takahashi, S., Yoshida, J., Takeo, M., Oikawa, J.,
707 Ohminato, T., Aoki, Y., Koyama, E., Tsuji, H., and Niwa, K.: High resolution imaging
708 in the inhomogeneous crust with cosmic-ray muon radiography: The density structure
709 below the volcanic crater floor of Mt. Asama, Japan, *Earth Planet. Sc. Lett.*, 263, 104–
710 113, 2007.

711

712 Tanaka, H. K. M., Uchida, T., Tanaka, M., Takeo M., Oikawa J., Ohminato T., Aoki Y.,
713 Koyama, E., Tsuji H.: Detecting a mass change inside a volcano by cosmic-ray muon
714 radiography (muography): First results from measurements at Asama volcano, Japan,
715 *Geophys. Res. Lett.*, GL039448, doi.org/10.1029/2009GL039448, 2009.

716

717 Tanaka, H. K. M., Miyajima, H., Kusagaya, T., Taketa, A., Uchida, T., and Tanaka, M.:
718 Cosmic muon imaging of hidden seismic fault zones: Raineater permeation into the
719 mechanical fracture zone in Itoigawa-Shizuoka Tectonic Line, Japan, *Earth Planet. Sc.*
720 *Lett.*, 306, 156–162, 2011.

721

722 Tanaka H.K.M., Kusagaya T., Shinohara H., Radiographic visualization of magma
723 dynamics in an erupting volcano, *Nat Commun.* 10, 5, 3381, doi: 10.1038/ncomms4381,
724 2014.

725

726 Tanaka, H. K. M.: Development of stroboscopic muography, *Geosci. Instrum. Method.*
727 *Data Syst.*, 2, 41–45, doi:10.5194/gi-2-41-2013, 2013.

728

729 Tanaka, H. K. M., Ohshiro, M.: Muographic data analysis method for medium-sized
730 rock overburden inspections, *Geosci. Instrum. Method. Data Syst.*, 5, 427–435,
731 doi:10.5194/gi-5-427-2016, 2016.

732

733 Tanaka H. K. M., Muraoka, H.: Interpreting muon radiographic data in a fault zone:
734 possible application to geothermal reservoir detection and monitoring, *Geosci. Instrum.*
735 *Method. Data Syst.*, 2, 145–150, <https://doi.org/10.5194/gi-2-145-2013>, 2013.

736

737 Varga D., Gál, Z., Hamar G., Molnár, J.S, Oláh, E. and Pázmándi, P.: Cosmic muon
738 detector using proportional chambers, *European Journal of Physics*, 36, 065006, 2015.

739

740 Varga D., Nyitrai, G., Hamar, G., Oláh, L., High Efficiency Gaseous Tracking Detector
741 for Cosmic Muon Radiography, *Advances in High Energy Physics*, 1962317,
742 <https://doi.org/10.1155/2016/1962317>, 2016.